

THE UNIVERSITY OF MIAMI

The Dynamic Structure of a Wind-Induced Eddy

BY

Thomas Stephen O'Keefe, Jr.

A THESIS

Submitted to the Faculty  
of the University of Miami  
in partial fulfillment of the requirements for  
the degree of Master of Science

Coral Gables, Florida

August 1971

Thesis  
0363

Thesis  
.0363

O'KEEFE, THOMAS STEPHEN, JR.

(M.S., Physical Oceanography)

The Dynamic Structure of a Wind-Induced Eddy. (August 1971).  
Abstract of a Master's Thesis at the University of Miami. Thesis  
supervised by Professor Claes Rooth.

The response of the ocean to an axisymmetric cyclone is investigated using a model based on the conservation of potential vorticity in the interior. The results, which confirm the conservation of potential vorticity, are used to obtain limiting values of the vertical eddy diffusivity and an effective Ekman depth. Some aspects of the response as a function of the horizontal wavenumber are also investigated. It is found that high wavenumber motion does not penetrate as deeply as low wavenumber motion.



THE UNIVERSITY OF MIAMI

The Dynamic Structure of a Wind-Induced Eddy

BY

Thomas Stephen O'Keefe, Jr.

A THESIS

Submitted to the Faculty  
of the University of Miami  
in partial fulfillment of the requirements for  
the degree of Master of Science

Coral Gables, Florida

August 1971

T143622

*[Faint, illegible text]*

*[Faint, illegible text]*

*[Faint, illegible text]*

*[Faint, illegible text]*

THE UNIVERSITY OF MIAMI

A thesis submitted in partial fulfillment of  
the requirements for the degree of  
Master of Science

Subject

The Dynamic Structure of a Wind-Induced Eddy

Thomas Stephen O'Keefe, Jr.





## ACKNOWLEDGEMENTS

During the time I studied at the School of Marine and Atmospheric Science, I was fortunate to develop lasting friendships with many people. I have also experienced a perceptible change in attitude toward science and have developed a sympathy for the problems of the scientist, and a respect for his motivation. The answer to the question "why" remains man's greatest challenge. The friendships made, and the change in perspective will be the most lasting and beneficial effects of the last two years.

I am indebted to the members of my thesis committee, Dr. Kamal Yacoub and Dr. Walter Düing. I am particularly grateful for the infinite patience of Dr. Claes Rooth, the committee chairman, who guided my efforts. I am thankful for the provocative advice of Dr. C.N.K. Mooers who gave me a particularly valuable commodity, his time.

Thanks are due Mr. Manuel Bascuas, who provided programming assistance, and Miss Linda Monaco, who typed the several drafts of the manuscript.

Finally, I thank my wife, Kathy, for understanding.

The financial support for this study was provided by the Office of Naval Research Contract No. N00014-67-A-0201-0013, Project No. NR 083-060.



## TABLE OF CONTENTS

	Page
LIST OF FIGURES . . . . .	v
LIST OF APPENDICES . . . . .	vi
I. INTRODUCTION . . . . .	1
II. METHODOLOGY . . . . .	5
III. DISCUSSION OF RESULTS . . . . .	12
A. Discussion of the Solution and Consistency of Results . . . . .	12
B. The Mixing Process and Momentum Transfer . . . . .	18
C. The Effect of Length Scale on Response . . . . .	22
D. Geostrophic Velocities . . . . .	25
IV. SUMMARY AND CONCLUSIONS . . . . .	29
APPENDIX . . . . .	31
LIST OF REFERENCES . . . . .	39



## LIST OF FIGURES

FIGURE	Page
1. The path of Hurricane Kara and stations of R/V PILLSBURY. Wind speed in knots is indicated . . . . .	2
2. The relation between density ( $\rho$ ), undisturbed depth ( $Z_0$ ) and stretching ( $\xi$ ) . . . . .	7
3. Observed mass structure of ocean after passage of Hurricane Kara. Isopleths are values of sigma-t ( $\sigma_t$ ) . . . . .	11
4. Comparison between the observed mass structure and the computed response after Hurricane Kara. $J_0(kr) = 0$ at 80 km . . . . .	13
5. Log-linear plot of temperature ( $^{\circ}\text{C}$ ) vs depth (m) . . . . .	19
6. Density difference ( $\text{gm/cm}^3$ ) plotted vs square of depth ( $\text{cm}^2$ ) for potential energy calculation. Station #24 is compared to the center of the computed curves . . . . .	21
7. Isopleths of stretching, $\xi(\text{m})$ , as a function of depth and length scale. Values of $\xi$ are normalized to 100 meters pumping at 25 meters matching depth . . . . .	24
8. Comparison of numerically calculated geostrophic velocities (cm/sec) with velocities found using the dynamic method (observed) . . . . .	27
9. $\phi = \text{constant}$ surface separated into horizontal and vertical components to illustrate coordinate transformation technique . . . . .	33



LIST OF APPENDICES

APPENDIX	Page
A. The Natural Coordinate System . . . . .	31
B. The Potential Vorticity Conservation Model . . . . .	34





## I. INTRODUCTION

In October of 1968, Tropical Storm Kara forced R/V PILLSBURY south from an operating area in the vicinity of latitude  $30^{\circ}25'N$ , longitude  $76^{\circ}52'W$ . While in the stages of maturation, the tropical storm displayed the curious behavior of slowing and crossing its own path several times. Kara eventually reached hurricane force, increased speed and moved on a generally northeast course. In transit to the operating area after passage of the storm, the research vessel experienced set to the right and then left, indicating that a hurricane-induced eddy had been crossed. Bathythermograph stations were taken in order to locate the associated dome-like density structure, and STD stations across the presumed dome were taken after it had been located. The track of Kara and the track of R/V PILLSBURY are shown in Figure 1. The hurricane track was obtained from the advisories issued by the National Hurricane Center.

Kara may be considered to have been quasi-stationary during the period 14-15 October 1968. Therefore it affords an opportunity to study some aspects of hurricane-induced dynamics through the upper part of the water column. As Stevenson (1966) points out, hurricanes are unique "laboratories" for the study of air-sea interaction and ocean dynamics. Although the significant atmospheric effects of a hurricane are spread over horizontal scales on the order of several hundred kilometers, the most interesting oceanic effects take place within an area which can be crossed in one day. Unfortunately,



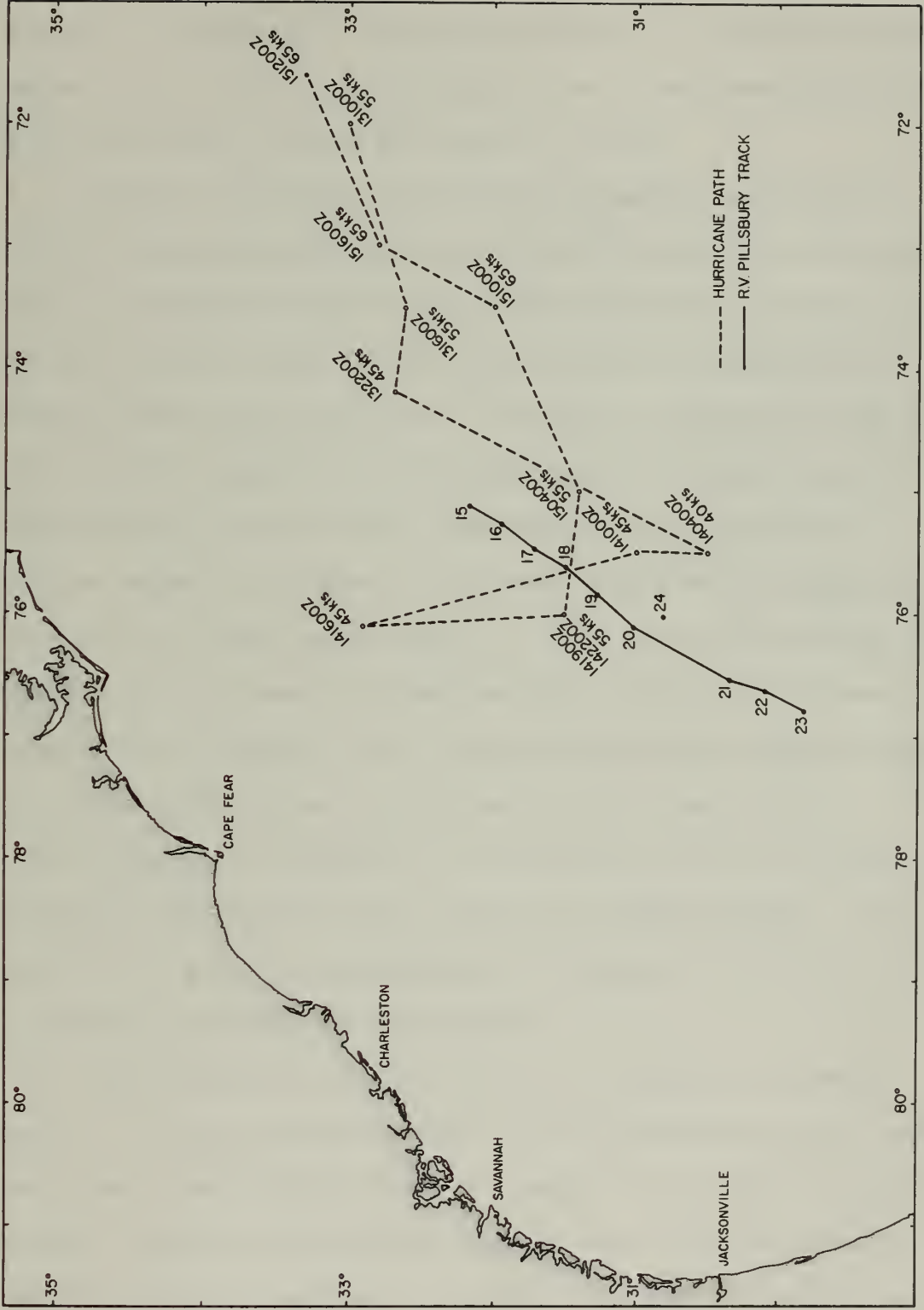


Figure 1. The path of Hurricane Kara and stations of R/V PILLSBURY. Wind speed in knots is indicated.



investigations of the response to hurricanes depend by necessity on "cruises of opportunity." Given the availability of research vessels, studies of this sort are further complicated by the unpredictability of the occurrence, duration and track of a storm.

A study of low intensity storms such as Kara is particularly relevant because the wind velocities are not too different from those found in the winter storms in the North Atlantic Ocean. In particular, the data provide a means of testing assumptions of conservation of potential vorticity in the ocean. An analysis of those areas where the conservation equations are not applicable is important because understanding the causes of the differences between observed and measured response contributes to an understanding of the response of the ocean in the near surface layer. A third reason for studying such storms is that the deep ocean response may be typical of numerous storms of near hurricane force. If so, the associated changes in mass structure are significant at great depths. For example, the perturbation of the isopycnals will have drastic effects on acoustic propagation at depths at least as great as the SOFAR channel. The analysis also serves as an addition to a catalogue of techniques useful in analyzing transient oceanic behavior.

Circular symmetry is assumed in the model used in this paper. However, it can be seen from Figure 1 that insufficient stations have been taken to positively identify the center of the vortex. Station 24 was made after the vortex had been crossed once, when the research vessel returned to take a center station. It was felt that the station was taken close to the center but the possibility that it was not



cannot be excluded. The stationarity of Kara increases the amplitude of the response. Since the data were collected several days after the storm passed, it may be assumed that most of the energy is found in geostrophic motion.





## II. METHODOLOGY

The existence of a cold water dome after the passage of a hurricane is suggestive of upwelling. This was concluded by Leipper (1967) and is supported by data collected by Landis (1966). Leipper's data inspired O'Brien and Reid (1967) to pursue their study of upwelling in a two layer ocean as a response to a stationary hurricane. O'Brien and Reid established through a transient, non-linear model that the wind stress associated with storms of hurricane force and structure is capable of producing velocity divergence in the surface layer and large scale upwelling. O'Brien (1967) added turbulent mixing to the model and produced results which bear resemblance to Leipper's observations of the near surface layer.

The problem can be approached somewhat differently. It is well known that surface divergence and associated upwelling will stretch water columns. A fluid will respond by spinning, thereby generating relative vorticity about the vertical axis. The effect extends to the bottom of the fluid and is transmitted much more efficiently than momentum transfer by friction. The model in this study utilizes the conservation of potential vorticity to describe the interior response. The assumption of a frictionless interior makes the continuously stratified problem tractable by allowing use of the conservation equation in the interior. This model and O'Brien's differ because they investigate different aspects of the response to axisymmetric forcing. O'Brien solves the governing equations numerically as an



initial value problem in time because he is interested in the evolution of the response. By its very nature, his two layer model is incapable of obtaining the structure of the interior. However, it is successful in duplicating many aspects of the time dependent response. This study seeks to model the steady-state response of the ocean independently of the generating mechanism using a realistic density profile.

The model used in this study was derived by Rooth (1970) and is presented fully in Appendix B. It makes use of the non-linear, time dependent equations of motion in deriving the vorticity equation. Hydrostatic equilibrium is assumed for the formation of the divergence equation. It is assumed that the data were collected a sufficient length of time after the storm passed to ensure that motion was essentially geostrophic. Combining the divergence equation and the vorticity equation results in a governing equation expressing the conservation of potential vorticity in a geostrophic velocity field,

$$\nabla^2 \xi + \frac{f^2}{N^2(Z_0)} \frac{\partial^2 \xi}{\partial Z_0^2} = 0. \quad \text{II-1}$$

$\xi$  is the lifting of a density surface from its undisturbed state (called the matching level),  $f$  is the Coriolis parameter, and  $N^2(Z_0)$  is the square of the Brunt-Väisälä frequency of the undisturbed state.  $Z_0$  is the geometric height in the undisturbed state. The observed mass distribution perturbed from the undisturbed state. The equation is the result of a transformation from cartesian coordinates with geometric height as the independent variable in the vertical to a "natural" coordinate system where density is the vertical coordinate. Figure 2 illustrates the relationship between  $\xi$  and  $Z_0$ . Geometric depth is the sum of  $Z_0$  and  $\xi$ . Formally,  $Z = Z_0(\rho) + \xi(Z_0, r)$ , where  $r$  is the radius.



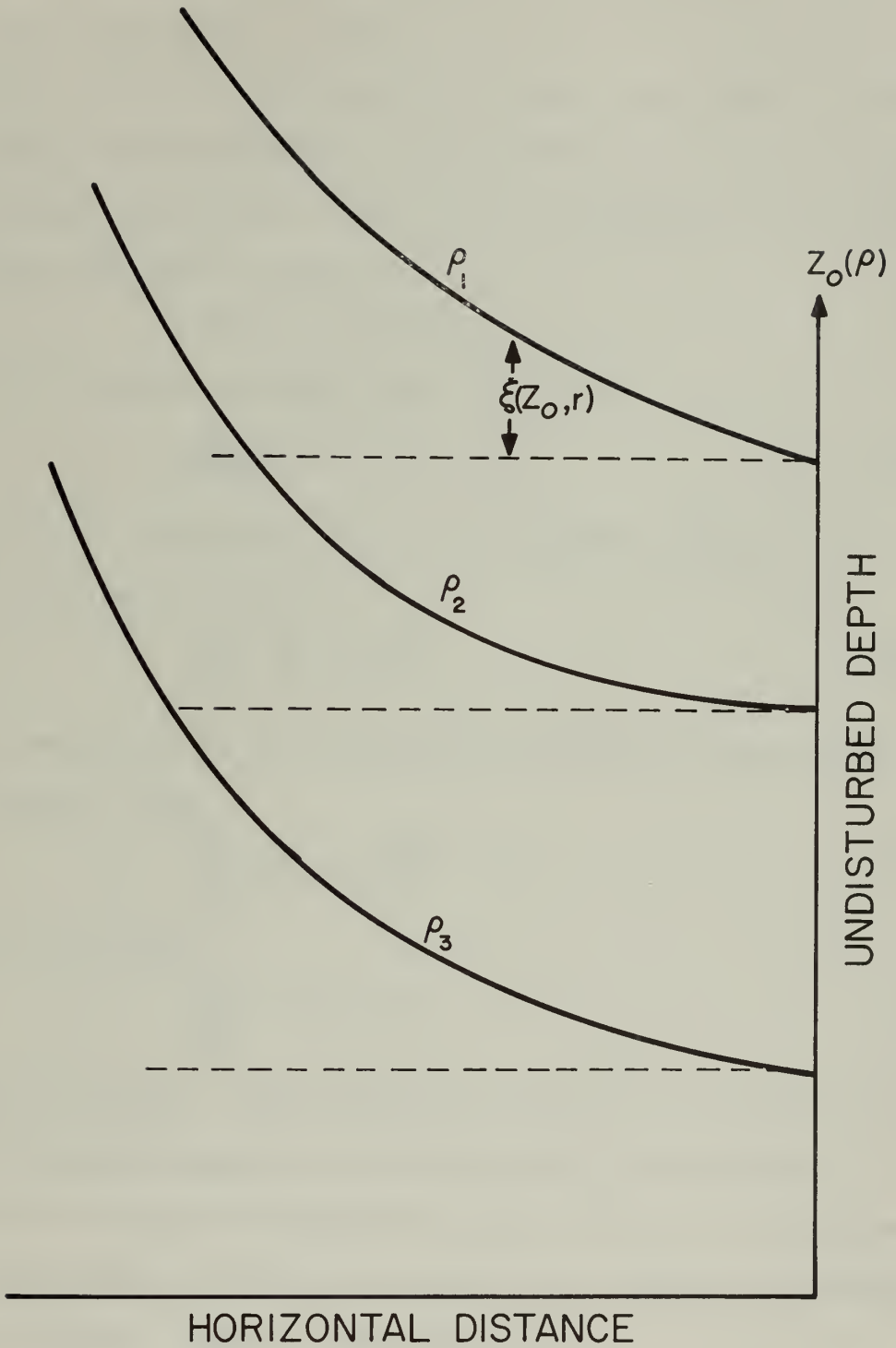


Figure 2. The relation between density ( $\rho$ ), undisturbed depth ( $Z_0$ ) and stretching ( $\xi$ ).



Not only is the numerical solution considerably simplified in this formulation, but solving in terms of the stretching is intuitively appealing. It is the stretching which generates the relative vorticity.

The horizontal Laplacian of  $\xi$  transforms directly from cartesian to cylindrical coordinates. Equation II-1 is therefore the governing equation in the latter system also. Let

$$\xi(Z_0, r) = R(r)Z(Z_0)$$

in order to separate variables, and II-1 becomes

$$\frac{f^2}{N^2(Z_0)} Z''R + Z\nabla^2R = 0. \quad \text{II-2}$$

For notational convenience,  $N^2(Z_0)$  will be written as  $N_0^2$ .

Rearranging II-2 yields

$$\frac{f^2}{N_0^2} \cdot \frac{Z''}{Z} = -\frac{\nabla^2R}{R}. \quad \text{II-3}$$

Since a function of  $Z_0$  can be equal to a function of  $r$  only if they are each constants, then

$$\frac{f^2}{N_0^2} \cdot \frac{Z''}{Z} = -\frac{\nabla^2R}{R} = k^2 \quad \text{II-4}$$

Equation II-4 implies

$$\frac{f^2}{N_0^2} Z'' - k^2Z = 0. \quad \text{II-5}$$

Equation II-5 must be solved numerically because of the inclusion of the Brunt-Väisälä frequency as a function of  $Z_0$ . Note that the selection of sign for the separation constant implies that solutions are sought which are exponential in form in the vertical and harmonic in the horizontal. Equation II-4 implies

$$\nabla^2R + k^2R = 0. \quad \text{II-6}$$

Writing the Laplacian in full, one obtains





$$R'' + \frac{R'}{r} + k^2 R = 0, \quad \text{II-7}$$

assuming axisymmetric motion. Equation II-7 is a form of Bessel's equation and has the solution

$$R = B J_0(kr) + C N_0(kr). \quad \text{II-8}$$

$N_0$  is a Neumann function or Bessel function of the second kind. Since the solution must be finite at  $r = 0$ , the constant  $C$  equals zero.

With no loss of generality, the radial solution is normalized to unit amplitude at  $r = 0$ . The separation, then, is the following:

$$\xi = \sum_{n=1}^{\infty} \xi_0(Z_0, 0) J_0(k_n r). \quad \text{II-9}$$

There is an infinity of solutions dependent on the value of  $k_n$ , the arbitrary constant of separation called the wavenumber. In the application of equation II-9 to this study, the solution can be reduced to the response to a single, dominant wavenumber. The technique will be discussed following a summary of the numerical method used to solve equation II-1.

Equation II-1 was solved numerically on the IBM 370/155 computer at the University of Miami. A pre-programmed scientific subroutine package was utilized which is a modification by Hamming of Milne's predictor-corrector method. Since the predictor-corrector method is not self-starting, a fourth order Runge-Kutta starting procedure is used to generate sufficient points (Ralston, 1965). The numerical method requires specification of  $\xi$  and  $\partial\xi/\partial Z_0$  as initial conditions. At the bottom the stretching of an isopycnal is zero. It is assumed that a dominant wavenumber for the disturbance exists in the interior. It will be shown later that this assumption is realistic. There are, then, two arbitrary parameters, wavenumber and slope at the bottom, which have to be determined. A solution for specific values of slope



and wavenumber can be obtained by devising a scheme which matches the numerical solution to the density structure in two dimensions. The matching uses up the two degrees of freedom associated with the arbitrary parameters. A numerical scheme could be devised which would optimize the matching process by some best fit method. It was felt, however, that a subjective graphical method was justified considering the quality of the data. The approach chosen was to select an intermediate density surface and vary the input to the computer program until the amplitude of the response and the decay of the  $J_0(kr)$  Bessel function matched the observed perturbation. Essentially, the numerical solution, generated as an initial value problem, was forced to meet conditions on a surface on which density is conserved.

The governing equation (II-1) requires the Brunt-Väisälä frequency of an undisturbed ocean as input. The input was taken from the temperature and salinity tables from R/V ATLANTIS stations 5446 and 5447 (Fuglister, 1960). The stations were selected because they display temperature-salinity characteristics fairly typical of the Sargasso Sea and are relatively unperturbed by local variations. Figure 3 shows the observed response of the ocean to the storm.



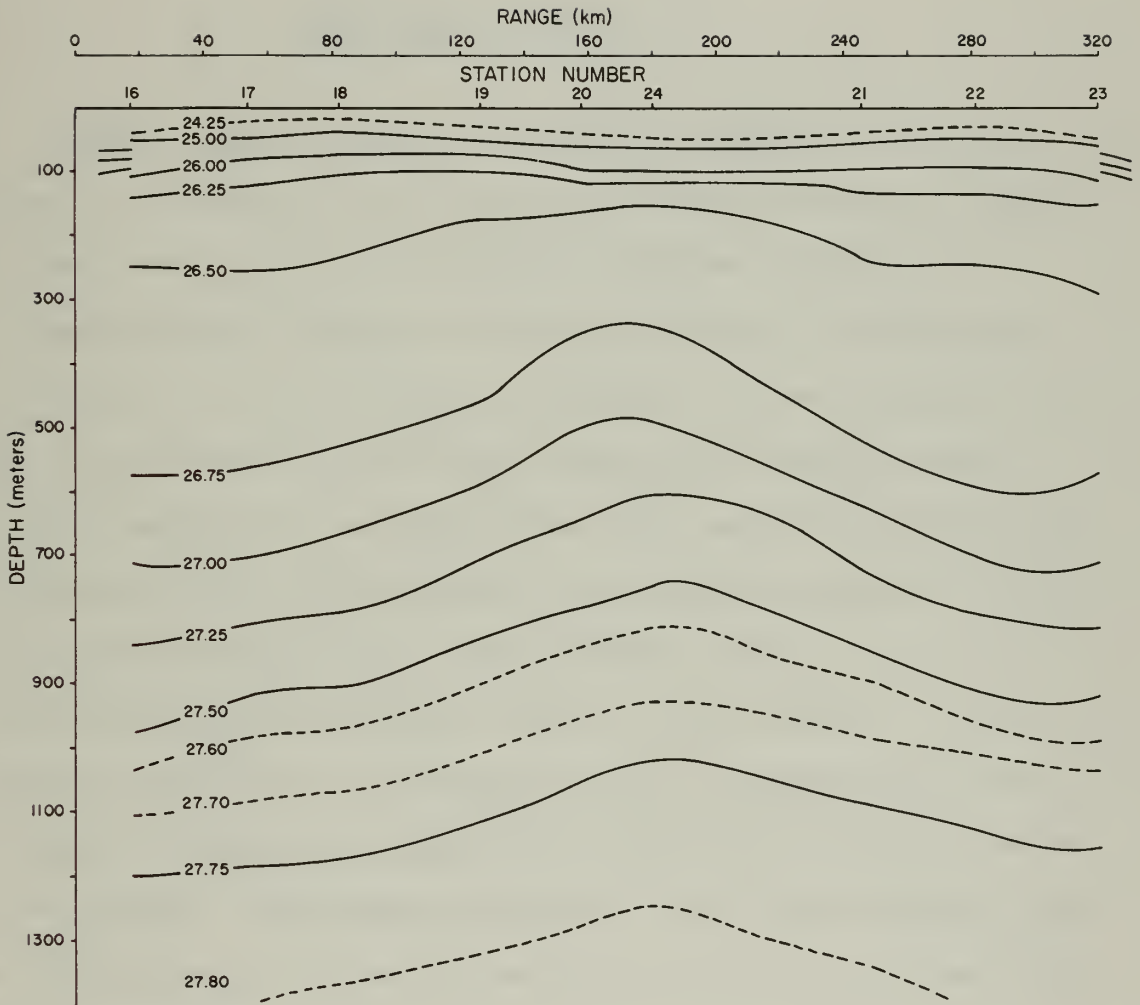


Figure 3. Observed mass structure of ocean after passage of Hurricane Kara. Isopleths are values of sigma-t ( $\sigma_t$ ).



### III. DISCUSSION OF RESULTS

#### A. DISCUSSION OF SOLUTION AND CONSISTENCY OF RESULTS

Figure 4 shows a comparison between the computed and observed curves. The observed mass distribution has been shifted to a common vertical axis. This step is consistent with the assumption of axisymmetric motion implied in the transformation of the Laplacian in equation II-6 to cylindrical coordinates. As seen in Figure 3, the axis of the observed curves slants slightly away from the vertical. With the exception of the near surface layer and a few isolated spots at the sides, where the assumption of axisymmetric motion is in doubt, the difference between the curves is no more than 10% of the total perturbation amplitude (trough to crest) of any isopycnal. In most cases the percentage is considerably lower. The cross-hatched area in Figure 4 indicates the areas where the deviation of the two curves is significant. Considerable flattening of the density surfaces occurs at least as deep as 230 meters, and there is no evidence of upwelling above 100 meters.

The lack of information about the state of the near surface layer prior to and during the storm precludes a complete analysis of the causes of the deviation between the two curves. According to Fuglister (1947), average surface temperatures for October in the area of the storm range from 25.8°C to 26.1°C. These temperatures correspond very well to the surface temperatures found after passage of Kara. If the





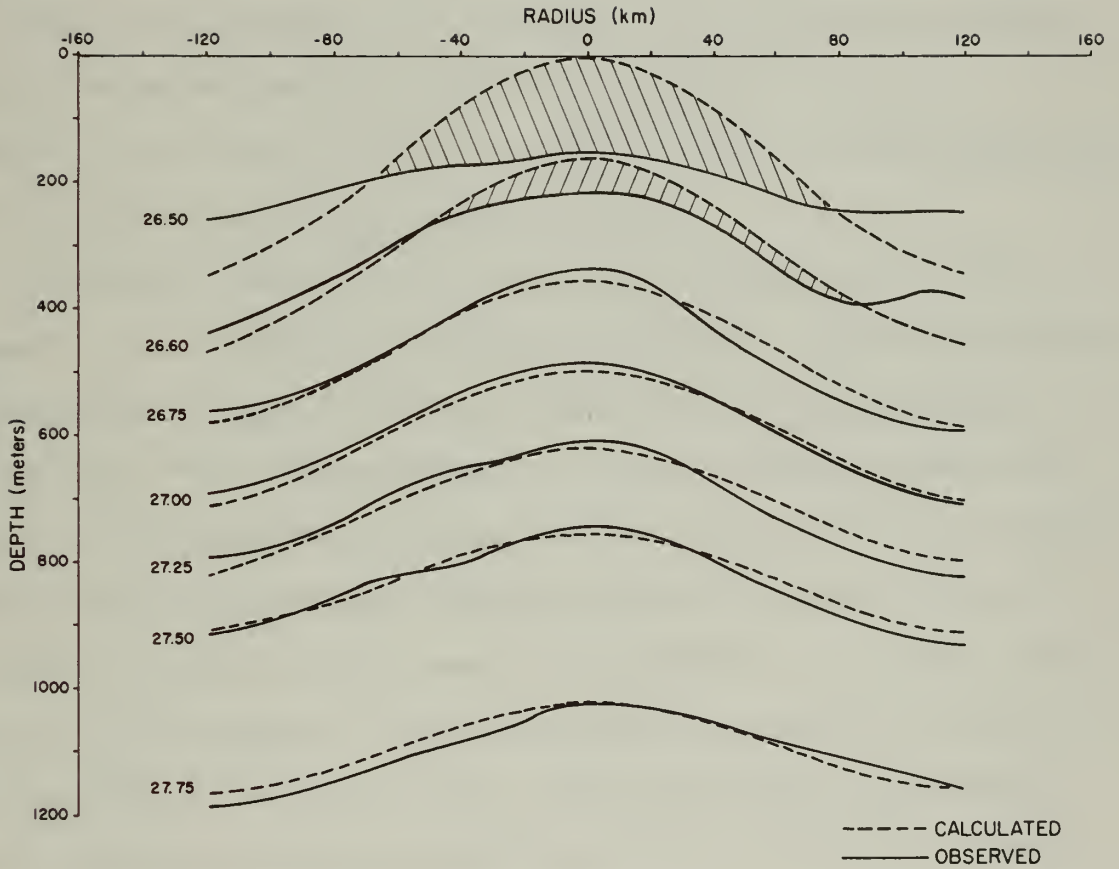


Figure 4. Comparison between the observed mass structure and the computed response after Hurricane Kara.  $J_0(kr) = 0$  at 80 km.



near surface layer did not cool significantly, then one must ask if upwelled water penetrated the thermocline and was mixed in the upper layer. It is possible that the apparent lack of surface cooling in the presence of obvious upwelling is the result of either horizontal advection in the surface layer moving the cold water away from the place of formation, or advection in the interior. The former is more likely, but the latter can partially explain the slanting of the axis of rotation of the vortex and the fact that the dome is located significantly to the south of the published hurricane track.

Upwelling clearly took place as a response to Kara. One would expect to find evidence of downwelling at the sides to satisfy continuity requirements. O'Brien (1967) finds downwelling in a numerical model and Leipper (1967) finds evidence of it from the changes in shape and depth of the thermocline. Surface data taken after Kara do not indicate downwelling. The mixed layer depth is remarkably constant across the vortex and is typical of the ocean in this region. At the sides of the vortex, in the interior, downwelling definitely occurred in balance of the upwelling in the center region. This can be seen by the dipping of the isopycnals below the undisturbed level. The disparity between the curves at the top of the pycnocline suggests significant downward penetration of momentum below the depth of the mixed layer, leading to an effective Ekman depth of about 230 meters. That is, if the Ekman layer is considered that region where friction effects dominate, and where the conservation equations are not applicable, then the depth of significant differences between the observed and computed curves may be identified as the Ekman depth.



It is possible to check the consistency of the results with existing ideas of surface wind stress by working backwards from the theoretical displacement of the isopycnals. The technique begins with the Ekman pumping relation

$$\rho fw = \text{curl } \tau, \quad \text{III-1}$$

where  $\rho$  is density,  $w$  is vertical velocity, and  $\tau$  is wind stress.

Stokes' theorem may be written as

$$\int_S \tau \cdot dS = \iint_A \text{curl } \tau \cdot dA, \quad \text{III-2}$$

or, by substituting equation III-1 for  $\text{curl } \tau$ , as

$$\int_S \tau \cdot dS = \rho \iint_A wf \cdot dA. \quad \text{III-3}$$

Assuming an axisymmetric wind stress distribution, equation III-3

becomes

$$\rho wf \pi r^2 = 2\pi r \tau, \quad \text{III-4}$$

or

$$\tau = wfr/2. \quad \text{III-5}$$

If  $w = \delta\xi/\delta t$  where  $\delta\xi$  is the displacement of the most perturbed density surface and  $\delta t$  is the time the storm was stationary, then the average stress distribution is

$$\bar{\tau} = \frac{\delta\xi \cdot f \cdot r}{2 \cdot \delta t}. \quad \text{III-6}$$

The average stress may be found by taking an average over the curve

$\xi = \xi_0 J_0(kr)$ . Then

$$\bar{\tau} = \frac{f}{2\pi} \cdot \frac{1}{R} \int_0^R \int_0^{2\pi} \frac{\xi \cdot r \cdot d\phi \cdot dr}{2 \cdot \delta t} \quad \text{III-7}$$

$$= \frac{f}{2\pi} \cdot \frac{\xi_0}{R} \int_0^R \int_0^{2\pi} \frac{J_0(kr) \cdot r \cdot d\phi \cdot dr}{2 \cdot \delta t}. \quad \text{III-8}$$

To simplify the integration, it was decided to utilize the series form



of the Bessel function:

$$J_0(Z) = 1 - \frac{Z^2}{2^2(1!)^2} + \frac{Z^4}{2^4(2!)^2} - \frac{Z^6}{2^6(3!)^2} + \dots \quad \text{III-9}$$

Noting that

$$\frac{1}{2\pi} \int_0^{2\pi} d\phi = 1,$$

and using

$$X = kr, \quad dr = dX/k$$

to change variables and integration limits, then III-8 becomes

$$\tau = \frac{\xi_0 \cdot f}{k^2 \cdot R} \int_0^{kr} \frac{X J_0(x) dX}{2 \cdot \delta t} \quad \text{III-10}$$

The dominant wavenumber found by matching the theoretical and observed curves is  $3.0 \times 10^{-5}$ . Therefore, the zero crossing occurs at  $r = 80$  km.

Using the well known relation

$$\bar{\tau} = \rho_a u_*^2 = \rho_w v_*^2 = C_D U_{10}^2 \cdot \rho_a \quad \text{III-11}$$

enables one to use the average stress calculated in equation III-10 to find wind velocity, or

$$U_{10}^2 = \frac{\bar{\tau}}{C_D \cdot \rho_a} \quad \text{III-12}$$

where  $u_*$  is the friction velocity in air,  $v_*$  is the friction velocity in water,  $\rho_a$  is the density of air ( $1.3 \times 10^{-3}$  gm cm<sup>-3</sup>),  $\rho_w$  is the density of water (1 gm cm<sup>-3</sup>),  $C_D$  is the drag coefficient, and  $U_{10}$  is the wind velocity at a specified height. The wind velocity is highly dependent on the choice of drag coefficient. Unfortunately, there are numerous estimates of the dependence of drag coefficients on wind speed and few agree. From Roll (1965) there seems to be a bunching of estimates for near hurricane force winds at  $C_D = 2.5 \times 10^{-3}$ . This is a figure O'Brien (1967) also uses and terms "classical." The results of this calculation for various values of the drag coefficient are





tabulated below.  $C_D = 1.5 \times 10^{-3}$  is a widely quoted value which Malkus and Riehl (1960) found worked well in their model.  $2.0 \times 10^{-3}$  is the mean of the two values.

$C_D$	$U_{10}(\text{KTS})$
$1.5 \times 10^{-3}$	57.6
$2.0 \times 10^{-3}$	50.2
$2.5 \times 10^{-3}$	45.2

Air Force penetrations of the storm during the time it was quasi-stationary found wind speeds between 45 and 55 knots. According to Colón (1966), the wind distribution in the lower few thousand feet is uniform, or nearly so. Therefore the wind speeds should be representative of those near the surface. The tabulated results of the calculations are inconclusive. One may say there is no inconsistency between the theoretical result and gathered data. Occasionally the results of theoretical models are used to fix parameters upon which the models critically depend. A definite statement cannot be made in this case. However, the results indicate that the drag coefficient probably falls within the above range for winds of near hurricane force.

As will be shown later in the paper, the penetration of the response of high wavenumber motion is less than that of lower wavenumbers due to the effect of the wavenumber on the exponential-like solution in the vertical (equation II-5). The ocean acts as a low-pass filter to the response. This means that the difference between the two curves at the level where they diverge significantly may be due partially to the effect of the response at higher wavenumbers, which will change the height of a density surface in some unknown fashion.



It is also possible that the presumed center of the vortex was not the exact center. If not, then missing the center can account for some of the difference between the curves.

#### B. THE MIXING PROCESS AND MOMENTUM TRANSFER

Several calculations can be made which place an upper limit on the effects of the mixing process. The calculations assume a balance in the vertical between the downward diffusion of heat due to mechanical mixing and the upwelling of cold water from below the local thermocline. The governing equation for this process is

$$w \cdot \partial T / \partial Z = \kappa \cdot \partial^2 T / \partial Z^2, \quad \text{III-13}$$

where  $w$  is vertical velocity,  $T$  is temperature and  $\kappa$  is the eddy diffusivity of heat. The solution of III-13 is

$$T = T_0 \exp(w/\kappa)Z. \quad \text{III-14}$$

$\kappa/w$  is the e-folding distance for the temperature decay and is therefore the scale height of the local thermocline in this problem.  $H_T$ , the thermocline scale height, may be found by taking the logarithm of III-14, obtaining the following:

$$\ln T = \ln T_0 + Z/H_T. \quad \text{III-15}$$

Plotting  $\ln T$  vs  $Z$  and finding the slope determines the scale height. Equation III-15 is the equation of a straight line on semi-log paper, and  $1/H_T$  is the slope of the line. Figure 5 is such a plot. Since pure mixing is assumed, the vertical velocity may be approximated by  $\delta h / \delta t$ , the difference in lifting between the observed and calculated curves divided by the relevant time scale of one day.  $\kappa$  determined in this manner is  $1400 \text{ cm}^2/\text{sec}$ . This value of  $\kappa$  is several orders of



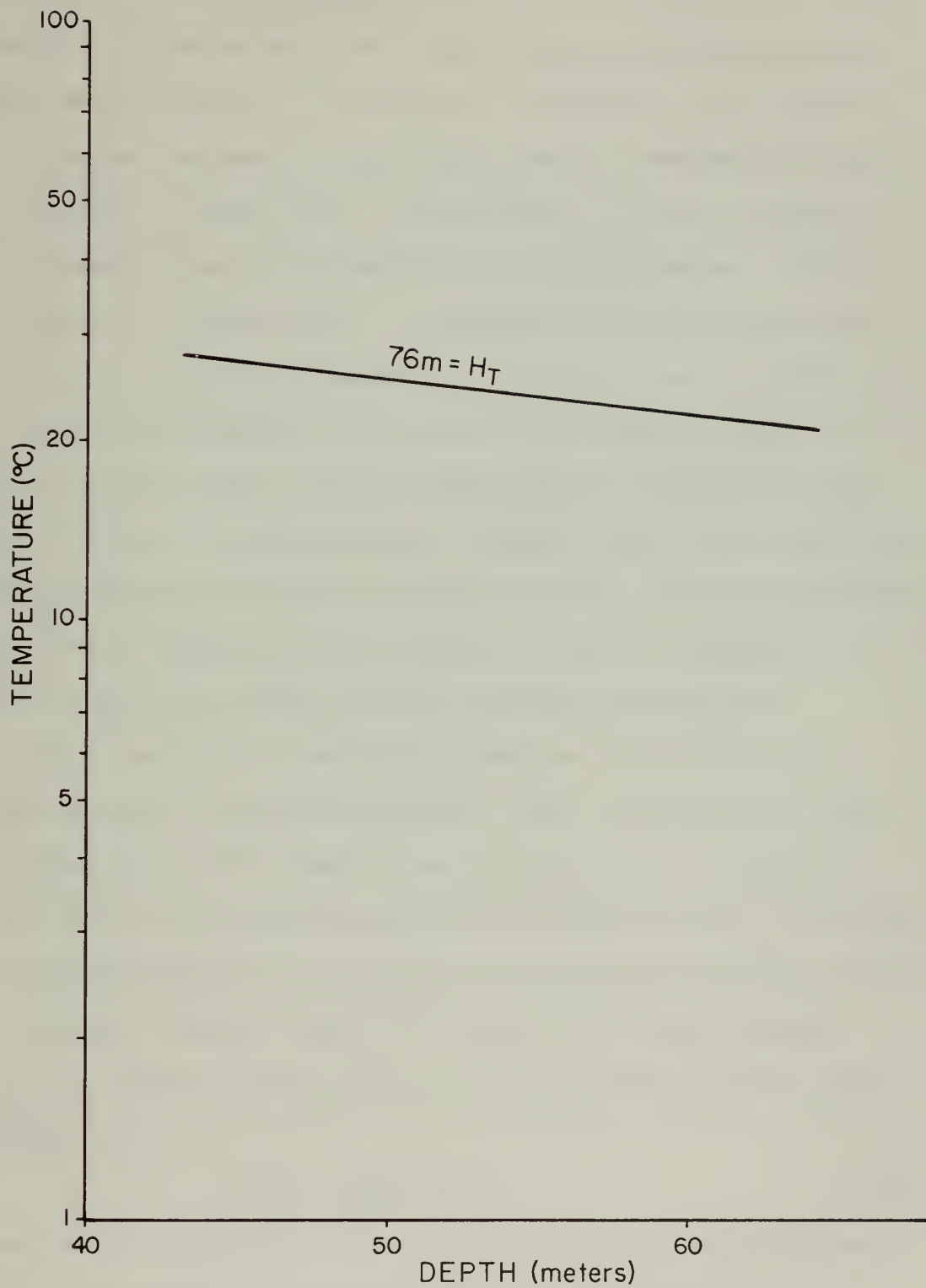


Figure 5. Log-linear plot of temperature (°C) vs depth (m).



magnitude too large for abyssal processes but is probably the correct order for surface processes where eddy viscosity and eddy diffusivity may be nearly the same. If the point of divergence of the curves is at 230 meters, the eddy viscosity found from the Ekman depth formula,  $d_0 = \pi\sqrt{2\nu/f}$ , is  $2000 \text{ cm}^2/\text{sec}$ .  $1400 \text{ cm}^2/\text{sec}$  is almost certainly an overestimate of the eddy diffusivity since Ekman divergence effects are neglected. If the depth of the mixed layer is neglected in the calculation of the eddy viscosity,  $d_0 = 180$  meters and  $\nu = 1200 \text{ cm}^2/\text{sec}$ . This calculation assumes the existence of two separate regimes: the mixed layer where eddy viscosity coefficients are very high; and the layer of Ekman divergence below the frictional layer, indicated by the disparity between observed and computed results. The similarity between the values of eddy viscosity and eddy diffusivity is presented for completeness and to suggest topics for further investigation.

Under conditions of negligible advection, it is possible to extend an energy calculation by Turner (1969). Assuming pure mixing, the change in potential energy between the observed and theoretical curves can be used to work backwards to find wind velocity. Selecting an isopycnal where the two curves do not diverge and calling the density  $\rho_0$  a reference density, one can plot  $\rho_z - \rho_0$  vs  $Z^2$  (depth squared). Taking one half the area under the resulting curve solves the energy equation,

$$E_{\text{POT}} = g \int (\rho_z - \rho_0) Z \, dZ, \quad \text{III-16}$$

graphically. Figure 6 is a plot of  $\Delta\rho$  vs  $Z^2$  for the center station, where maximum upwelling occurred. The change in potential energy found planimetrically is  $10.14 \times 10^7 \text{ ergs cm}^{-2}$ . By dimensional arguments,





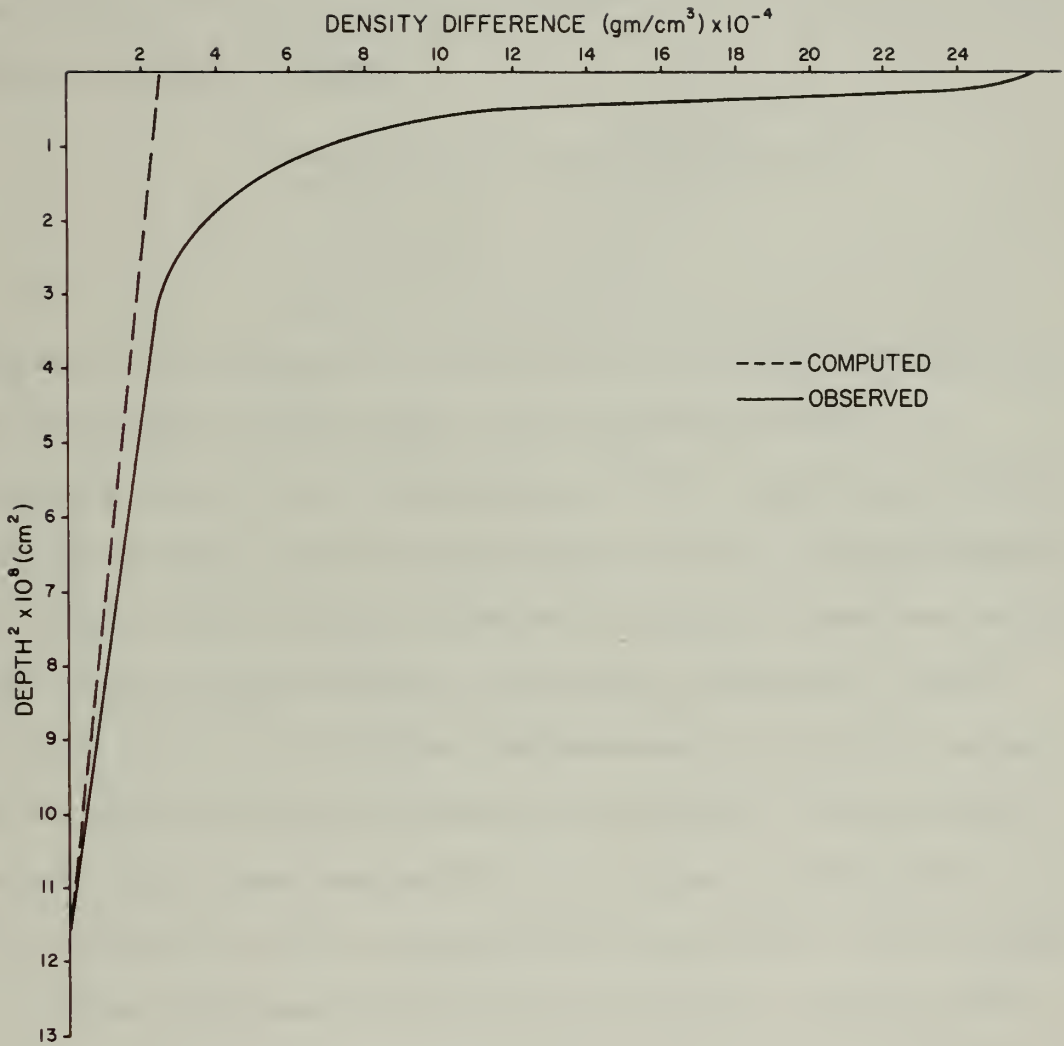


Figure 6. Density difference (gm/cm<sup>3</sup>) plotted vs square of depth (cm<sup>2</sup>) for potential energy calculation. Station #24 is compared to the center of the computed curves.



Turner asserts that it is reasonable to write the time rate of change of energy as

$$\frac{dE_{\text{POT}}}{dt} = C_1 \tau U_{10} = C_2 \rho U_{10}^3. \quad \text{III-17}$$

The tabulation below gives values of wind speed for two values of the constant  $C_2$  found by Turner.

$C_2$	$U_{10}$ (KTS)
$2.6 \times 10^{-8}$	71.4
$1.3 \times 10^{-8}$	90

Both values of wind speed are too high if pure mixing is responsible for the potential energy change. If one accepts 50 knots as a reasonable value of wind speed during the storm, then surface mixing accounts for about half the energy change. That is, at least half of the density field discrepancy from the theoretical curves must derive from the deep Ekman divergence. As the drag coefficient, Turner's constants are not well defined. The dependence of Turner's constants and the drag coefficient on wind speed is unknown. Turner's method requires a one-dimensional process and a regime in which surface cooling and resultant convective overturning are unimportant. Both processes are usually significant under hurricane conditions, although their effect may be minimal in this case since surface cooling apparently did not occur. Selecting the center station minimizes the advective effects, since  $\xi$  is a maximum there and  $\partial\xi/\partial r$  approaches zero. As Turner correctly points out, his method is illustrative but hardly conclusive.

### C. THE EFFECT OF LENGTH SCALE ON RESPONSE

Some interesting properties of the solution as a function of scale



of forcing and depth are illustrated in Figure 7. The governing equation (II-1) was solved using the same initial conditions and density profile but different values of wavenumber. The length scale was determined by selecting the value of radius which corresponded to the first zero of the  $J_0$  Bessel function, found from the formula  $(1/\text{wavenumber}) \times 2.4$ . The values of  $\xi$  were normalized to 100 meters of Ekman pumping at  $Z_0 = 25$  meters and isopleths of constant  $\xi$  were plotted. The response may be split into a barotropic and baroclinic regime. In the barotropic regime, response is characterized by the stretching being a linear function of depth, since stretching is proportional to vertical velocity.

The transition from a baroclinic to a barotropic response is rather broad in scale, occurring between 300 to 500 km. For scales greater than 500 km, the response may be continued to be barotropic. The response for high wave numbers is confined to a shallow surface layer. The latter provides the rationale for basing the solution of the vorticity equation on the existence of a dominant wavenumber in the interior. The dependence of the vertical structure of the response on the scale of the motion suggests a definite problem in the representation of a continuously stratified ocean by a two-layer model. For the higher wavenumbers, the two layer model lacks sufficient resolution to describe the response adequately.

The ordinate in Figure 7 is undisturbed depth ( $Z_0$ ). Since depth is equal to the sum of the undisturbed depth and the stretching, zero depth in the figure should not be confused with the free surface. The free surface lies considerably below  $Z_0 = 0$ .

It is anticipated that similar diagrams can be generated using



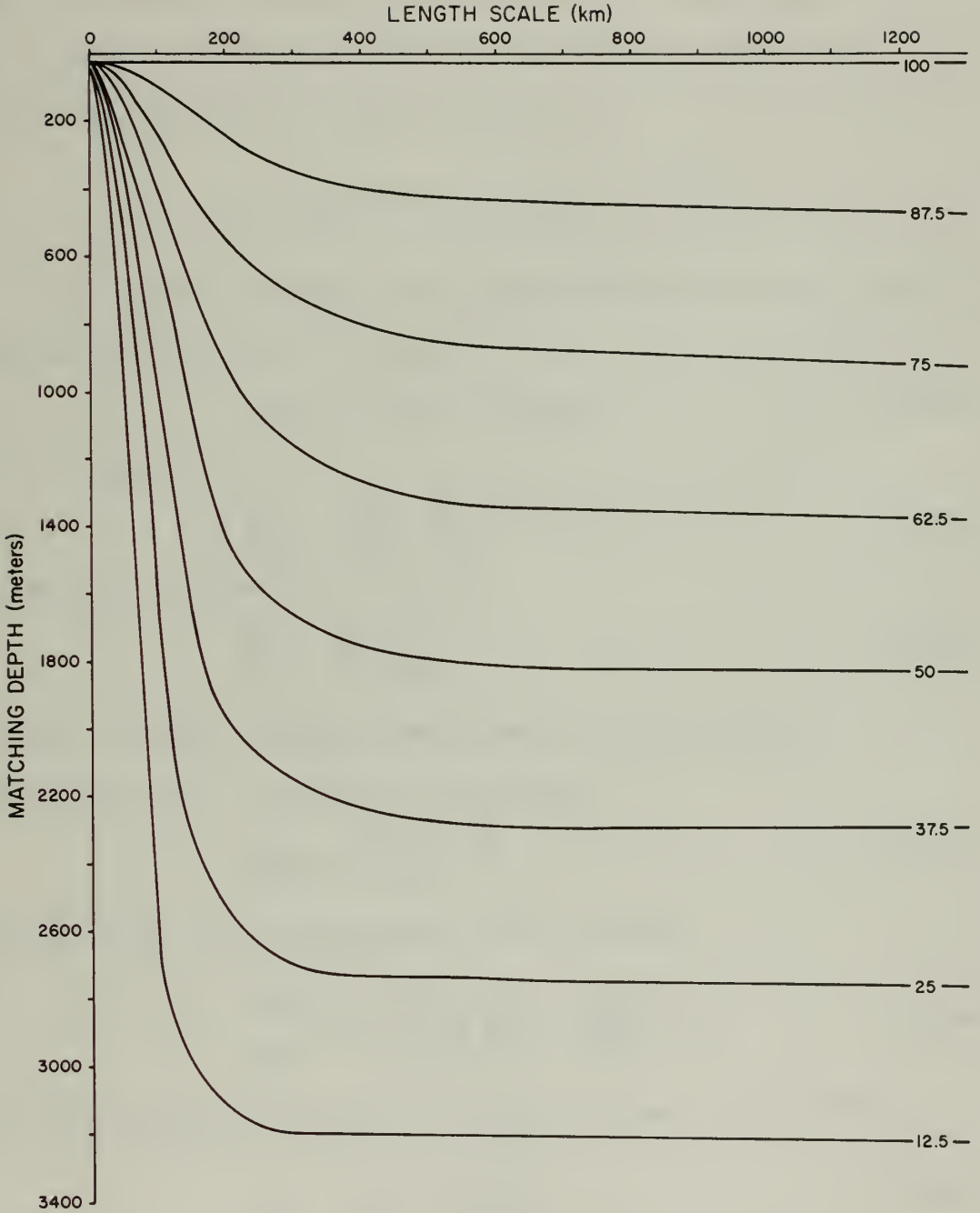


Figure 7. Isopleths of stretching,  $\xi$  (m), as a function of depth and length scale. Values of  $\xi$  are normalized to 100 meters pumping at 25 meters matching depth.





density distributions typical of other areas of the ocean. The diagrams should prove useful in predicting the response in these areas. A density profile with higher resolution than that obtained from Fuglister's Atlantic Ocean Atlas is preferable.

#### D. GEOSTROPHIC VELOCITIES

It is possible to calculate geostrophic velocities using the solution of equation II-1. Noting

$$Z(\rho, r) = Z_0(\rho) + \xi(Z_0, r), \quad \text{III-20}$$

and from Appendix A,

$$\left. \frac{\partial \rho}{\partial r} \right|_{Z_0} = - \left. \frac{\partial Z}{\partial r} \right|_{\rho} \frac{\partial \rho}{\partial Z_0}, \quad \text{III-21}$$

one may use the thermal wind equation,

$$\frac{\partial U}{\partial Z_0} = \frac{-g}{\rho f} \left. \frac{\partial \rho}{\partial r} \right|_{Z_0}, \quad \text{III-22}$$

to find velocities throughout the column and for any radius.

Substituting III-21 into III-22, one obtains

$$\frac{\partial U}{\partial Z_0} = \frac{g}{\rho f} \left. \frac{\partial Z}{\partial r} \right|_{\rho} \frac{\partial \rho}{\partial Z_0}. \quad \text{III-23}$$

Equation III-23 may be integrated in the vertical:

$$\int_{U_{Z_0''}}^{U_{Z_0'}} dU = \frac{1}{f} \int_{Z_0''}^{Z_0'} \frac{g}{\rho} \frac{\partial \rho}{\partial Z_0} \cdot \left( \frac{\partial Z}{\partial r} \right)_{\rho} dZ_0. \quad \text{III-24}$$

Noting  $U_{Z_0''}$  (bottom) = 0 and  $N_0^2 = \frac{-g}{\rho} \frac{\partial \rho}{\partial Z_0}$ , equation III-24 becomes

$$U_{Z_0'} = -\frac{1}{f} \int_{Z_0''}^{Z_0'} N_0^2 \left( \frac{\partial Z}{\partial r} \right)_{\rho} dZ_0. \quad \text{III-25}$$

Introduce III-20 for Z in III-25, obtaining

$$U_{Z_0'} = -\frac{1}{f} \int_{Z_0''}^{Z_0'} N_0^2 \cdot \left( \frac{\partial \xi}{\partial r} \right)_{\rho} dZ_0. \quad \text{III-26}$$

Geostrophic velocities were calculated numerically using equation III-26



and the result established previously,  $\xi = \xi_0 J_0(kr)$ . The derivative of  $\xi$  is

$$\partial\xi/\partial r = k \xi_0 J_1(kr). \quad \text{III-27}$$

Equation III-26 is a valid expression for the velocities induced by Kara, except in the Ekman layer, where the predicted density field departs from the observed. Veronis (1956) showed that motion which has forcing on scales larger than the baroclinic radius of deformation is essentially geostrophic. In this case, the scale of forcing, 80 km, is more than twice the baroclinic radius of deformation, 36 km. Figure 8 is a comparison of the geostrophic velocities based on equation III-26 and velocities calculated using the dynamic method (called the observed velocities). The reference level for calculating the observed velocities was found using Defant's method. The level was conspicuously present in all the profiles. Although the percentage of error is high at the lower depths, the absolute magnitude difference is low. In general, the magnitude of error remains the same as depth decreases. The two velocity profiles agree rather well in magnitude and general shape. Aside from the reasons for the difference between the curves in the Ekman layer, which have been discussed, the calculation of geostrophic velocities poses special problems. In this case, the distances between stations used to calculate the velocities by the dynamic method were extreme. It was found that velocities at a given radius and depth varied as much as 5 cm/sec depending on the particular combination of stations used. The curves represent the smoothest combination. The observed velocities were computed from the non-centered observed data, which certainly accounts for some of the difference between the curves. The effect of centripetal acceleration has been



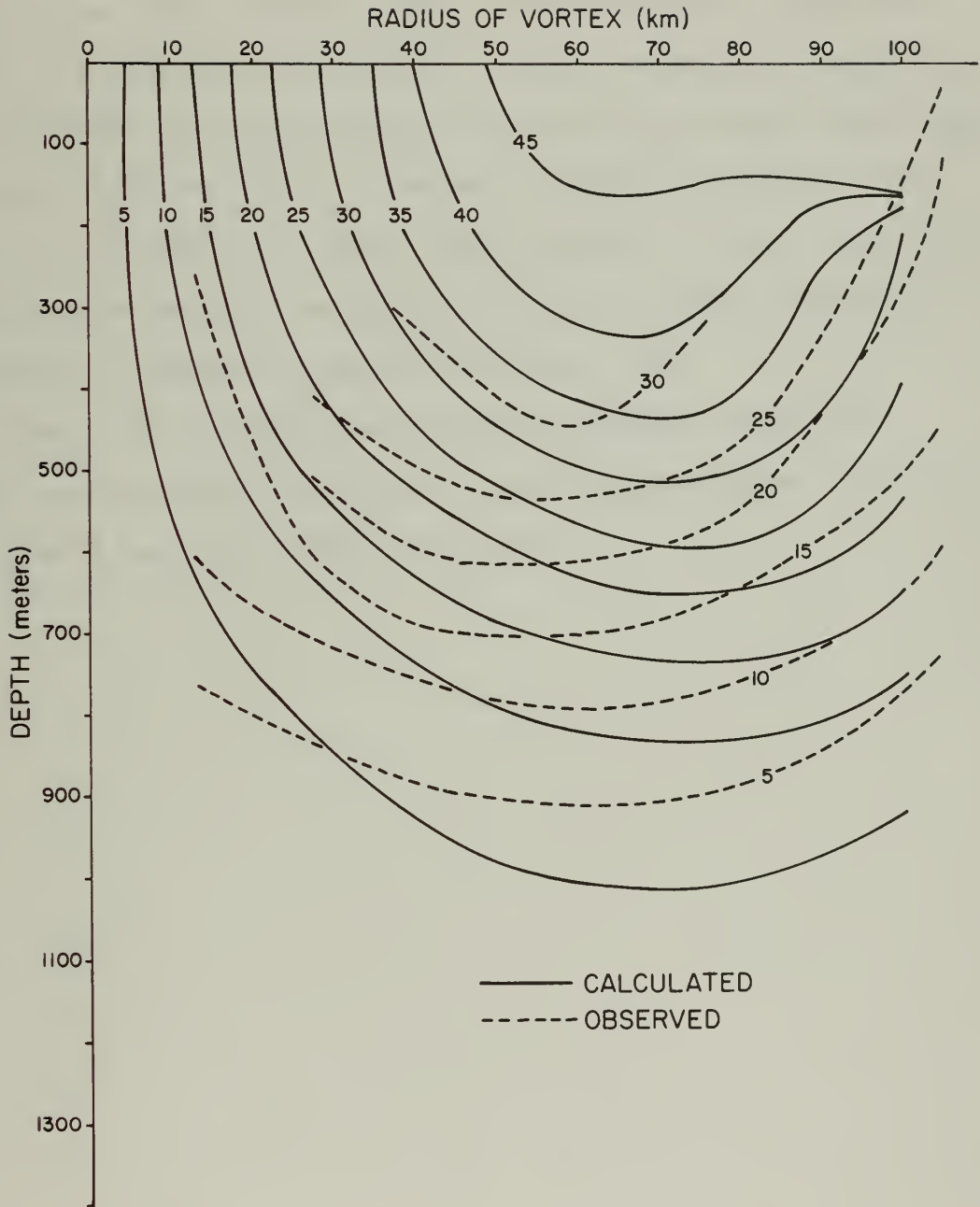


Figure 8. Comparison of numerically calculated geostrophic velocities (cm/sec) with velocities found using the dynamic method (observed).



neglected in the calculation of velocities, and in the formulation of the vorticity conservation model. The inclusion of centripetal accelerations makes the model non-linear, introducing an undesired degree of difficulty in solving the vorticity equation. A measure of the importance of the centrifugal force term is the Rossby number,  $\frac{v}{f \cdot r}$  (Neumann and Pierson, 1966). Choosing  $r = 40$  km,  $v = 40$  cm/sec, and  $f = 7.5 \times 10^{-5} \text{ sec}^{-1}$ , the Rossby number is 0.13. It can be shown that geostrophic velocity is an overestimate of the gradient velocity if curvature is important (Haltiner and Martin, 1957).

The success in obtaining substantial agreement between the theoretical mass field and velocities and the observations supports the validity of the initial model formulation.





#### IV. SUMMARY AND CONCLUSIONS

A model based on the conservation of potential vorticity was solved numerically. The solution was utilized to investigate some aspects of the oceanic response to a tropical storm as a function of horizontal scale. In particular, the interior response of a moderately intense, quasi-stationary cyclone was duplicated. The matching was successful below a depth of 230 meters which was associated with the Ekman depth. The lack of information concerning the state of the ocean in the near-surface layer prior to the passage of Hurricane Kara compounded the problem of discovering what caused the divergence of the observed and computed curves. The divergence was attributed to the neglect of high wavenumber modes when solving for the interior response, and to some ill-defined combination of vertical mixing and momentum transfer by friction. Gross estimates indicate that the two processes are of equal importance in this particular case. An upper limit for the eddy diffusivity is  $1400 \text{ cm}^2/\text{sec}$ . Vigorous mixing, if it occurred, may not have resulted in significant cooling of the mixed layer.

Geostrophic velocities were calculated from the raw data using Defant's method to find a reference level of no motion. These velocities were compared to those calculated from the numerical solution. The velocities agree rather well below the near-surface layer. Since the velocity computation integrates the stretching, the comparison of velocities should not be expected to be as successful as the comparison of  $\xi$  itself. The integration of  $\xi$  means that errors are accumulated



over the entire column. Geostrophic vertical shear matches better than geostrophic velocities. It is plausible that the nearly constant error in magnitude between the velocity fields is a result of inaccuracies in the dynamic computations; specifically, limitations in the Defant method of obtaining the level of no motion may be the cause.

It was found that the scale of forcing can have dramatic effects on the penetration of the response. For equal Ekman pumping, higher wavenumber (short scale) response does not penetrate very deep into the ocean compared to low wavenumber response. Thus the scale of the disturbance must be considered when choosing the depth and number of layers for modelling a continuously stratified fluid. A two layer model may lack the resolution necessary to accurately describe the response in the upper layer. Adequate modelling of the near-surface layer by a model such as the one used in this study requires the inclusion of high wavenumber motion.



## APPENDIX A

## THE NATURAL COORDINATE SYSTEM



Although the standard cartesian coordinate system is the one normally used in hydrodynamics, there is no reason why the vertical coordinate must be geometric height, a fact recognized long ago by meteorologists and some oceanographers. The use of a "natural" vertical coordinate, such as pressure, density or potential density, can simplify an analysis but render boundary conditions formidable.

In the potential vorticity conservation model, density will be utilized as the "natural" vertical coordinate. This is advantageous because it enables one to solve directly for the displacement of an isopycnal from equilibrium. The method of coordinate transformation is discussed in Haltiner and Martin (1957). It is summarized below since the method is implied in the model and is used directly in deriving the geostrophic velocities (equation III-26).

Consider  $\phi(x,y,z,t) = \text{constant}$ . The change of  $\eta(x,y,z,t)$  along  $\phi = \text{constant}$  is equal to the change along the horizontal plus the change along the vertical due to the slope of  $\phi$ , i.e. From Figure 9,

$$\delta\eta)_{a-c} = \delta\eta)_{a-b} + \delta\eta)_{b-c}. \quad \text{A-1}$$

Now,

$$\delta\eta)_{y,\phi,t_0} = \frac{\partial\eta}{\partial x})_{y,z,t_0} \delta x + \frac{\partial\eta}{\partial z})_{x,y,t_0} \delta z \quad \text{A-2}$$

by the chain rule at a constant time,  $t_0$ . A-2 may be written as

$$\frac{\partial\eta}{\partial x})_{y,\phi,t_0} = \frac{\partial\eta}{\partial x})_{y,z,t_0} + \frac{\partial\eta}{\partial z})_{x,y,t_0} \frac{\partial z}{\partial x})_{y,\phi,t_0}, \quad \text{A-3}$$

where  $\frac{\partial z}{\partial x}$  is the slope of the  $\phi$  surface in the x direction. Let  $\eta = \rho$  and A-3 becomes

$$\frac{\partial\rho}{\partial x})_z = \frac{\partial\rho}{\partial x})_\phi - \frac{\partial\rho}{\partial z} \cdot \frac{\partial z}{\partial x}. \quad \text{A-4}$$





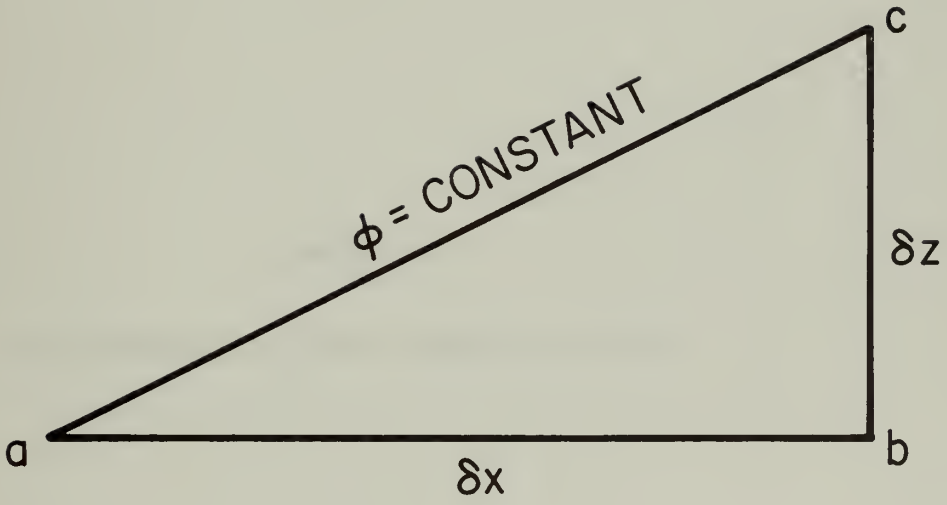


Figure 9.  $\phi = \text{constant}$  surface separated into horizontal and vertical components to illustrate coordinate transformation technique.



## APPENDIX B

## THE POTENTIAL VORTICITY CONSERVATION MODEL



The governing equation for the interior motion of a hurricane, it is hypothesized, expresses the conservation of potential vorticity. The equations of motion used are non-linear, time dependent, hydrostatic equations in a rotating system characterized by the Coriolis parameter,  $f$ , which is a function of the horizontal coordinates alone:

$$u_t + \bar{u} \cdot \nabla u - fv + \pi_x = 0 \quad \text{B-1}$$

$$v_t + \bar{u} \cdot \nabla v + fu + \pi_y = 0, \quad \text{B-2}$$

where  $\pi \equiv \frac{p}{\rho} + gz$ . The vorticity equation may be formed by cross-differentiating equations B-1 and B-2, resulting in B-3:

$$\left[ \frac{\partial}{\partial t} + u \frac{\partial}{\partial x} + v \frac{\partial}{\partial y} \right] (v_x - u_y) + (f + v_x - u_y)(u_x + v_y) + uf_x + vf_y = 0 \quad \text{B-3}$$

B-3 may be written as

$$\left[ \frac{\partial}{\partial t} + u \frac{\partial}{\partial x} + v \frac{\partial}{\partial y} \right] (f + v_x - u_y) + (f + v_x - u_y)(u_x + v_y) = 0, \quad \text{B-4}$$

since  $f$  is not a function of time. That is,

$$\frac{d}{dt} (f + v_x - u_y) + (f + v_x - u_y)(u_x + v_y) = 0, \quad \text{B-5}$$

where

$$\frac{d}{dt} \equiv \frac{\partial}{\partial t} + u \frac{\partial}{\partial x} + v \frac{\partial}{\partial y}.$$

The divergence equation may be formed by taking  $\frac{\partial}{\partial x}$  (equation B-4) and adding to  $\frac{\partial}{\partial y}$  (equation B-2).

$$\frac{d}{dt} (u_x + v_y) - f(v_x - u_y) + \nabla^2 \pi + f_y u - f_x v + u_x^2 + v_y^2 + v_x u_y + u_y v_x = 0 \quad \text{B-6}$$

Assuming geostrophic motion reduces the balance equation to

$$f(v_x - u_y) = \nabla^2 \pi. \quad \text{B-7}$$

The continuity equation is

$$u_x + v_y + w_z = 0. \quad \text{B-8}$$

In the vertical,  $w$  depends only on  $z(\rho)$ , therefore



$$(u_x + v_y) + \frac{\partial w}{\partial \rho} \cdot \frac{\partial \rho}{\partial z} = 0.$$

Noting  $w \equiv dz/dt$ , equation B-8 becomes

$$\frac{\partial z}{\partial \rho}(u_x + v_y) + \frac{d}{dt}\left(\frac{\partial z}{\partial \rho}\right) = 0. \quad \text{B-9}$$

Substitute equation B-9 into the vorticity equation (B-4) to obtain

$$\frac{d}{dt}(f + v_x - u_y) - (f + v_x - u_y) \cdot \frac{\frac{d}{dt}(\partial z / \partial \rho)}{\partial z / \partial \rho} = 0. \quad \text{B-10}$$

Rearranging terms, equation B-10 becomes

$$\frac{\frac{d}{dt}(f + v_x - u_y)}{f + v_x - u_y} - \frac{\frac{d}{dt}(\partial z / \partial \rho)}{\partial z / \partial \rho} = 0, \quad \text{B-11}$$

or, by definition of the logarithm,

$$\frac{d}{dt} \left( \frac{v_x - u_y + f}{\partial z / \partial \rho} \right) = 0. \quad \text{B-12}$$

Equation B-12 implies that for each fluid element

$$\frac{v_x - u_y + f}{\partial z / \partial \rho} = \text{constant}. \quad \text{B-13}$$

The existence of a uniform reference state implies that the constant is a function of density alone. If the reference state is rest, relative vorticity is zero, and the constant,  $\phi(\rho)$ , equals  $f/(\partial z / \partial \rho)_0$ . The vorticity equation, then, becomes

$$\frac{v_x - u_y + f}{\partial z / \partial \rho} = \frac{f}{(\partial z / \partial \rho)_0}. \quad \text{B-14}$$

Substituting equation B-7 into B-12 and rearranging, one obtains

$$\left( \frac{1 + \nabla^2 \pi}{f^2} \right) \left( \frac{\partial z}{\partial \rho} \right)_0 = \frac{\partial z}{\partial \rho}. \quad \text{B-15}$$

Next, apply the hydrostatic equation,

$$\pi = \frac{P}{\rho} + gz. \quad \text{B-16}$$

Rearranging and taking the partial derivative with respect to  $z$  results in

$$\frac{\partial}{\partial z}(\pi - gz)\rho = P_z. \quad \text{B-17}$$





Assuming hydrostatic equilibrium, B-17 becomes

$$\frac{\partial}{\partial z}(\pi - gz)\rho = -g\rho. \quad \text{B-18}$$

Integrating B-18 results in the following:

$$\rho\pi - \rho gz = \rho_0 \pi_0 - \int_0^z \rho g dz. \quad \text{B-19}$$

The last term in equation B-19 can be integrated by parts:

$$-\int_0^z \rho g dz = -\rho gz + \int_{\rho_0}^{\rho} g z d\rho. \quad \text{B-20}$$

Substituting B-20 into B-19, the desired forms of the hydrostatic equation is achieved:

$$\pi = \pi_0 + \frac{1}{\rho} \int_{\rho_0}^{\rho} g z d\rho. \quad \text{B-21}$$

Take the Laplacian of B-21:

$$\nabla^2 \pi = \nabla^2 \pi_0 + \frac{1}{\rho} \int_{\rho_0}^{\rho} g \nabla^2 z d\rho. \quad \text{B-22}$$

Substitute equation B-22 into equation B-15:

$$\frac{\partial z}{\partial \rho} - \left( \frac{\partial z}{\partial \rho} \right)_0 = \frac{1}{f^2} (\nabla^2 \pi_0 + \frac{1}{\rho} \int_{\rho_0}^{\rho} g \nabla^2 z d\rho) \left( \frac{\partial z}{\partial \rho} \right)_0.$$

Therefore, if  $\rho_0$  is chosen as the surface density, where  $h$  is the free surface height,

$$\frac{\partial z}{\partial \rho} - \left( \frac{\partial z}{\partial \rho} \right)_0 = \frac{g}{f^2} (\nabla^2 h + \frac{1}{\rho} \int_{\rho_0}^{\rho} \nabla^2 z d\rho) \left( \frac{\partial z}{\partial \rho} \right)_0. \quad \text{B-23}$$

The depth,  $z$ , may be split into two parts,

$$z = Z(\rho) + \xi(x, y, z_0).$$

Equation B-23 becomes, then, after rearranging,

$$\nabla^2 h + \frac{1}{\rho} \int_{\rho_0}^{\rho} \nabla^2 \xi d\rho = \frac{f^2}{g} \frac{\partial \xi}{\partial \rho} \left( \frac{\partial \rho}{\partial z} \right)_0. \quad \text{B-24}$$

Next, take the derivative of B-24 with respect to  $\rho$ :

$$\frac{1}{\rho} \nabla^2 \xi = \frac{f^2 \rho_0}{g \rho_0} \left( \frac{\partial \xi}{\partial \rho} \right) \left( \frac{\partial \rho}{\partial z} \right)_0 = \frac{f^2 \rho_0}{g \rho_0} \frac{\partial}{\partial \rho} \left( \frac{\partial \xi}{\partial z} \right). \quad \text{B-25}$$



Recall

$$\frac{\partial}{\partial \rho} \equiv \left( \frac{\partial z}{\partial \rho} \right)_0 \frac{\partial}{\partial z_0} ,$$

so equation B-25 becomes

$$\frac{1}{\rho_0} \nabla^2 \xi = \frac{-f^2}{\rho_0 N^2(z_0)} \frac{\partial^2 \xi}{\partial z_0^2} ,$$

or

$$\nabla^2 \xi + \frac{f^2}{N^2(z_0)} \frac{\partial^2 \xi}{\partial z_0^2} = 0. \quad \text{B-26}$$

Equation B-26 is the governing equation used in the analysis described

in the text. The basic derivation is attributed to Rooth (1970).

Several steps were expanded by this author for clarity and completeness.



**LIST OF REFERENCES**



- CHOQUET-BRUHAT, Y., 1967. Problems and Solutions in Mathematical Physics. Holden-Day, Inc., San Francisco, 314 pp.
- COLÓN, J., 1966. Some aspects of Hurricane Carla (1961). Hurricane Symposium, American Society for Oceanography, Houston, 1-33.
- FISHER, E.L., 1958. Hurricanes and the sea surface temperature field. Journal of Meteorology, 15 (3) : 328-333.
- FORMIN, L.M., 1964. The Dynamic Method in Oceanography. Elsevier Publishing Company, New York, 212 pp.
- FUGLISTER, F.C., 1947. Average monthly sea surface temperatures of the western North Atlantic Ocean. Papers in Physical Oceanography and Meteorology, 10 (2) : 1-25.
1960. Atlantic Ocean Atlas. Woods Hole Oceanographic Institution, Woods Hole, 209 pp.
- GEISLER, J.E., 1970. Linear theory of the response of a two layer ocean to a moving hurricane. Geophysical Fluid Dynamics, 1 (2) : 249-272.
- HALTINER, G.J., AND F.L. MARTIN, 1957. Dynamic and Physical Meteorology. McGraw-Hill, New York, 470 pp.
- INTERNATIONAL BUSINESS MACHINES, 1968. SYSTEM/360 Scientific Subroutine Package (360A-CM-03X), IBM, White Plains, 454 pp.
- KRAUS, E.B., AND C. ROOTH, 1961. Temperature and steady state heat flux in the ocean surface layers. Tellus, 13 (2) : 231-238.
- KRAUS, E.B., AND J.S. TURNER, 1967. A one-dimensional model of the seasonal thermocline. I. A laboratory experiment and its interpretation. Tellus, 19 (1) : 88-97.
- LANDIS, R.C., 1966. Synoptic analysis of near surface and subsurface temperatures in the Atlantic Ocean following Hurricane Betsy. Texas A & M Technical Report 66-30-T, College Station, 37 pp.
- LEIPPER, D.F., 1966. Influence of the hurricane on the structure of the thermocline, II. Hurricane Symposium, American Society for Oceanography, Houston, 173-188.
1967. Observed ocean conditions and Hurricane Hilda. Journal of the Atmospheric Sciences, 24 (2) : 182-196.
- MALKUS, J.S., AND H. RIEHL, 1960. On the dynamics and energy transformations in steady-state hurricanes. Tellus, 12 (1) : 1-20.
- MALKUS, J.S., 1962. Large scale interactions. The Sea, Vol. I, M.N. Hill, Ed., Interscience, London, 88-294.





- McCALLA, T.R., 1967. Introduction to Numerical Methods and FORTRAN Programming. John Wiley and Sons, Inc., New York, 359 pp.
- NEUMANN, G., AND W.J. PIERSON, JR., 1966. Principles of Physical Oceanography. Prentice-Hall, Inc., London, 545 pp.
- O'BRIEN, J.J., AND R.O. REID, 1967. The non-linear response of a two-layer, baroclinic ocean to a stationary, axially-symmetric hurricane: Part I. Upwelling induced by momentum transfer. *Journal of the Atmospheric Sciences*, 24 (2) : 197-207.
- O'BRIEN, J.J., 1967. The non-linear response of a two-layer, baroclinic ocean to a stationary, axially-symmetric hurricane: Part II. Upwelling and mixing induced by momentum transfer. *Journal of the Atmospheric Sciences*, 24 (2) : 208-215.
- PHILLIPS, O.M., 1966. The Dynamics of the Upper Ocean. Cambridge University Press, London, 261 pp.
- RALSTON, A., 1965. A First Course in Numerical Analysis. McGraw-Hill, New York, 578 pp.
- ROLL, H.U., 1965. Physics of the Marine Atmosphere. Academic Press, New York, 426 pp.
- ROOTH, C., 1970. Potential vorticity conservation model. (personal communication)
- STOMMEL, H., K. SAUNDERS, W. SIMMONS AND J. COOPER, 1969. Observations of the diurnal thermocline. *Deep Sea Research, Supplement to Volume 16*, 269-284.
- TURNER, J.S., AND E.B. KRAUS, 1967. A one-dimensional model of the seasonal thermocline. II. The general theory and its consequences. *Tellus*, 19 (1) : 98-105.
- TURNER, J.S., 1969. A note on wind mixing at the seasonal thermocline. *Deep Sea Research, Supplement to Volume 16*, 297-300.
- VERONIS, G., 1956. Partition of energy between geostrophic and non-geostrophic oceanic motions. *Deep Sea Research*, 3 (3) : 157-177.



## VITA

LT. Thomas Stephen O'Keefe, Jr., USN, was born in Orange, New Jersey on 21 June 1944. His parents are Thomas Stephen O'Keefe and Jane Phillips O'Keefe. He received his elementary education in Our Lady of Sorrows Grammar School, South Orange, New Jersey, and his secondary education in Columbia High School, Maplewood, New Jersey. In June 1962, he entered the U.S. Naval Academy, Annapolis, Maryland. Upon graduation in June 1966, with a Bachelor of Science degree, he was commissioned an Ensign in the U.S. Navy. Subsequent naval service included two years in the Destroyer Force of the Atlantic Fleet, and one year as Officer-in-Charge of a patrol craft in South Vietnam.

He was admitted to the Graduate School of the University of Miami in September 1969. He was granted the degree of Master of Science in August 1971.

Permanent address: 955 Greenbrier Road  
Hagerstown, Maryland 21740



21 AUG 74  
1 SEP 75  
4 MAR 80

22024  
23166  
25700

Thesis 131795  
0363 O'Keefe  
The dynamic struc-  
ture of a wind-induced  
eddy.

21 AUG 74  
1 SEP 75  
4 MAR 80

22024  
23166  
25700

T  
0

Thesis 131795  
0363 O'Keefe  
The dynamic struc-  
ture of a wind-induced  
eddy.

thes0363

The dynamic structure of a wind-induced



3 2768 001 96947 0

DUDLEY KNOX LIBRARY